

# Primary Crystallization Phases and Magnetic Property of FeZrB Alloys

Yu Wanqiu<sup>1,2</sup>, Lu Liping<sup>1</sup>, Zuo Bin<sup>2</sup>

<sup>1</sup> School of Materials Science and Engineering, Changchun University of Science and Technology, Changchun 130022, China; <sup>2</sup> National Demonstration Center for Experimental Physics Education, Jilin Normal University, Siping 136000, China

**Abstract:** A series of FeZrB alloys with different nominal composition were prepared by melt-spinning and then annealed at their first crystallization temperatures. The thermal curve, microstructure and magnetic property of the alloys were investigated by simultaneous thermal analyzer (STA), X-ray diffraction (XRD), transmission electron microscopy (TEM) and vibrating sample magnetometer (VSM). The results show that the primary crystallization phases are different with the composition of FeZrB alloys changing. Four groups of primary crystallization phases can be observed in the alloys, i.e.  $\alpha$ -Fe phase,  $\alpha$ -Fe+Fe<sub>12</sub>Si<sub>2</sub>ZrB type phases,  $\alpha$ -Fe+ $\alpha$ -Mn type phases and  $\alpha$ -Fe+Fe<sub>2</sub>B+ZrB phases, and their morphologies are different observed by TEM. The relations of saturation magnetization ( $M_s$ ) and coercivity ( $H_c$ ) for the alloys with different primary crystallization phases are as follows:  $M_{s(\alpha\text{-Fe})} > M_{s(\alpha\text{-Fe}+\alpha\text{-Mn type})} > M_{s(\alpha\text{-Fe}+\text{Fe}_2\text{B}+\text{ZrB})} > M_{s(\alpha\text{-Fe}+\text{Fe}_{12}\text{Si}_2\text{ZrB-type})}$  and  $H_{c(\alpha\text{-Fe}+\alpha\text{-Mn type})} > H_{c(\alpha\text{-Fe}+\text{Fe}_2\text{B}+\text{ZrB})} > H_{c(\alpha\text{-Fe}+\text{Fe}_{12}\text{Si}_2\text{ZrB-type})} > H_{c(\alpha\text{-Fe})}$ , respectively.

**Key words:** FeZrB alloys; primary crystallization phases; microstructure; saturation magnetization; coercivity

Fe-based amorphous and nanocrystalline soft materials are widely used in the field of power electronics and electrical engineering due to their excellent soft magnetic performance. Their magnetic property and microstructures have been extensively investigated over the past few decades<sup>[1-4]</sup>.

Fe-based nanocrystalline soft materials with excellent soft magnetic property can be obtained by annealing the amorphous precursor into the composites of  $\alpha$ -Fe nanograins surrounded by an amorphous layer (namely two-phase nanocrystalline structure). However, besides bcc  $\alpha$ -Fe phase, other kinds of nanocrystalline phases have also been observed in the primary crystallization processes of Fe-based alloys. Structure transformations of Fe-B-Si, Fe-P-C, Fe-P-B-C alloy systems with various additions have been investigated by I. V. Lyasotskii and N. B. Dyakonova et al.<sup>[5-8]</sup> They reported that many metastable phases at the initial stage of devitrification, such as  $\pi$ -phase,  $\chi$ -phase,  $\sigma$ -phase and  $H$ -phase, have tetrahedrally close packed (TCP) or aperiodic structures. It is noteworthy that the  $\pi$ -phase and  $\chi$ -phase are

the  $\beta$ -Mn type and  $\alpha$ -Mn type phases, respectively, which can also be found in the Fe-Mo-(Cr)-C<sup>[9-11]</sup> and Fe-Si-C<sup>[12]</sup> amorphous alloy systems. In addition, the Cr<sub>23</sub>C<sub>6</sub>-type metastable Fe<sub>23</sub>B<sub>6</sub> phase can be observed in the Fe-B-C-(Si)<sup>[13]</sup>, Fe-Nb-B<sup>[14]</sup> and Fe-Ni-Nb-B<sup>[15]</sup> amorphous alloy systems, and metastable  $\chi$ -Cr<sub>6</sub>Fe<sub>18</sub>Mo<sub>5</sub> and  $M_7C_3$  phases can be seen in the Fe<sub>50</sub>Cr<sub>15</sub>Mo<sub>14</sub>C<sub>15</sub>B<sub>6</sub> amorphous alloy<sup>[16]</sup>. Furthermore, other  $\alpha$ -Mn type<sup>[17-20]</sup>,  $\beta$ -Mn type<sup>[20, 21]</sup>,  $\sigma$ -phase<sup>[12]</sup>, Fe<sub>23</sub>B<sub>6</sub>-type<sup>[22-24]</sup> and  $\chi$ -FeCrMo-like<sup>[25]</sup> structure phases can be observed in other Fe-based alloy systems.

NANOPERM Fe-Zr-B alloy system is one of the important systems for Fe-based soft magnetic alloys, and it can meet the demands for green energy-saving and environmental protection in preparation and application. However, to handle multicomponent alloys with more than three elements is complicated. To mitigate this issue, many researches on Fe-Zr-B alloy system have been employed<sup>[26-32]</sup>, and the primary crystallization phases of FeZrB alloys have been analyzed<sup>[29-32]</sup>.

Received date: May 2, 2019

Foundation item: National Natural Science Foundation of China (51301075); Technology Studying Project of "13th five-year" Office of Education of Jilin Province (2017)

Corresponding author: Lu Liping, Ph. D., Professor, School of Materials Science and Engineering, Changchun University of Science and Technology, Changchun 130022, P. R. China, Tel: 0086-431-85583147, E-mail: luliping771219@126.com

Copyright © 2020, Northwest Institute for Nonferrous Metal Research. Published by Science Press. All rights reserved.

In this work, different kinds of primary crystallization phases were observed in the FeZrB alloys with 76 at%~85 at% Fe. The diagram of different primary crystallization phases for FeZrB alloys was given. The influence of composition changes on the microstructure of alloys was explored, and the relationship between the microstructure and magnetic properties of alloys with different primary crystallization phases were established. This work can help to effectively design composition of alloy to obtain materials with excellent soft magnetic performance.

## 1 Experiment

FeZrB alloy ribbons with nominal compositions of  $\text{Fe}_{93-x}\text{Zr}_7\text{B}_x$  ( $x=8, 9, 10, 12, 14, 15$ ),  $\text{Fe}_{81}\text{Zr}_8\text{B}_{11}$ ,  $\text{Fe}_{91-x}\text{Zr}_9\text{B}_x$  ( $x=10, 12, 15$ ),  $\text{Fe}_{79.5}\text{Zr}_{10}\text{B}_{10.5}$  and  $\text{Fe}_{76}\text{Zr}_{12+x}\text{B}_{12-x}$  ( $x=0, 3$ ) were prepared using a single-roller melt-spinning equipment in an Ar atmosphere with a copper wheel rotating at a surface velocity of 38 m/s.

The thermal curve was measured by simultaneous thermal analyzer (STA, 449F5). According to the STA curves, the as-quenched ribbons were annealed at the first crystallization temperature under vacuum conditions. Structural characterizations of samples were analyzed by X-ray diffraction (XRD, D/max 2500/PC, Cu-K $\alpha$ ,  $\lambda=0.15406$  nm) and transmission electron microscopy (TEM, JEM-2100E). Grain size ( $D$ ) of  $\alpha$ -Fe was calculated by Scherrer equation  $D=0.89\lambda/\beta\cos\theta$  ( $\lambda$  is the X-ray wavelength,  $\beta$  is the width of half-height diffraction peak, and  $\theta$  is the Bragg angle). Saturation magnetization ( $M_s$ ) and coercivity ( $H_c$ ) were investigated by vibrating sample magnetometer (VSM, Lake Shore M7407).

## 2 Results and Discussion

Fig.1 shows the XRD patterns of as-quenched FeZrB alloys with different nominal compositions. No crystalline peaks are observed in the as-quenched alloys of  $\text{Fe}_{93-x}\text{Zr}_7\text{B}_x$  ( $x=8, 9, 10, 12, 14, 15$ ),  $\text{Fe}_{81}\text{Zr}_8\text{B}_{11}$ ,  $\text{Fe}_{91-x}\text{Zr}_9\text{B}_x$  ( $x=10, 12, 15$ ),  $\text{Fe}_{79.5}\text{Zr}_{10}\text{B}_{10.5}$  and  $\text{Fe}_{76}\text{Zr}_{12}\text{B}_{12}$ . For the  $\text{Fe}_{76}\text{Zr}_{15}\text{B}_9$  alloy in the as-quenched state, the amorphous,  $\alpha$ -Fe and  $\alpha$ -Mn type phases can be observed.

Fig.2 shows the STA traces of as-quenched FeZrB alloys with different nominal compositions. The number and location of crystallization peaks are different from each other. The STA traces of  $\text{Fe}_{93-x}\text{Zr}_7\text{B}_x$  ( $x=8, 9, 10$ ) alloys are similar to each other and the first crystallization peak is low and flat, as shown in Fig.2a. With increasing the B and Zr contents, the crystallization behavior changes and the first crystallization peak sharpens, as shown in Fig.2b and 2c. For  $\text{Fe}_{76}\text{Zr}_{15}\text{B}_9$  and  $\text{Fe}_{76}\text{Zr}_{12}\text{B}_{12}$  alloys, the temperatures of the first crystallization peak are higher than those of other alloys, as shown in Fig.2d.

The as-quenched alloy ribbons were annealed at the first crystallization temperature and the corresponding

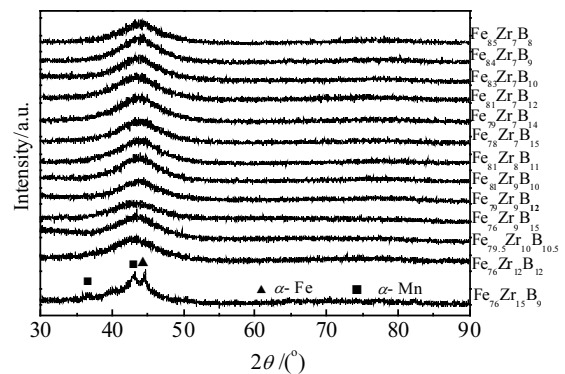


Fig.1 XRD patterns of as-quenched FeZrB alloys with different nominal composition

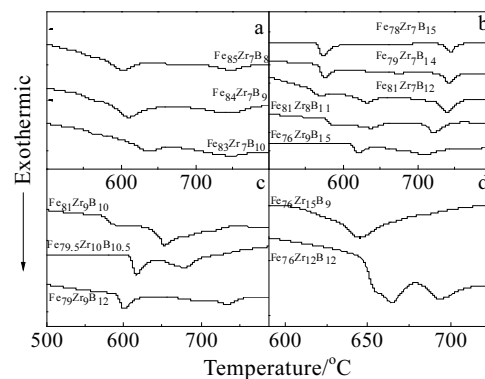


Fig.2 STA traces of as-quenched FeZrB alloys with different nominal composition

XRD patterns are shown in Fig.3. Compared with XRD patterns of as-quenched FeZrB alloys, those of the  $\text{Fe}_{93-x}\text{Zr}_7\text{B}_x$  ( $x=8, 9, 10$ ) alloys obviously show the characteristic peak corresponding to  $\alpha$ -Fe phase, as shown in Fig.3a. The characteristic peaks can verify that the  $\text{Fe}_{12}\text{Si}_2\text{ZrB}$  type phase appears as the primary crystallization phase besides  $\alpha$ -Fe phase in  $\text{Fe}_{93-x}\text{Zr}_7\text{B}_x$  ( $x=12, 14, 15$ ),  $\text{Fe}_{81}\text{Zr}_8\text{B}_{11}$  and  $\text{Fe}_{76}\text{Zr}_9\text{B}_{15}$  alloys, as shown in Fig.3b. In addition, the  $\alpha$ -Mn type phase exists in the  $\text{Fe}_{91-x}\text{Zr}_9\text{B}_x$  ( $x=10, 12$ ) and  $\text{Fe}_{79.5}\text{Zr}_{10}\text{B}_{10.5}$  alloys together with  $\alpha$ -Fe phase as the primary crystallization phase (Fig.3c). For  $\text{Fe}_{76}\text{Zr}_{15}\text{B}_9$  and  $\text{Fe}_{76}\text{Zr}_{12}\text{B}_{12}$  alloys, the primary crystallization phases consist of  $\alpha$ -Fe phase,  $\text{Fe}_2\text{B}$  and ZrB (Fig.3d). The primary crystallization phases are different with the composition of FeZrB alloys changing. All XRD patterns can be divided into four groups according to the primary crystallization phases.

Fig.4 gives the diagram of primary crystallization phases for FeZrB alloys with 76 at%~85 at% Fe (It is noteworthy that the alloy composition is nominal). The atomic radius of Fe, Zr and B is 0.124, 0.159 and 0.098 nm, and the electro negative of Fe, Zr and B is 1.83, 1.33 and 2.04, respectively.

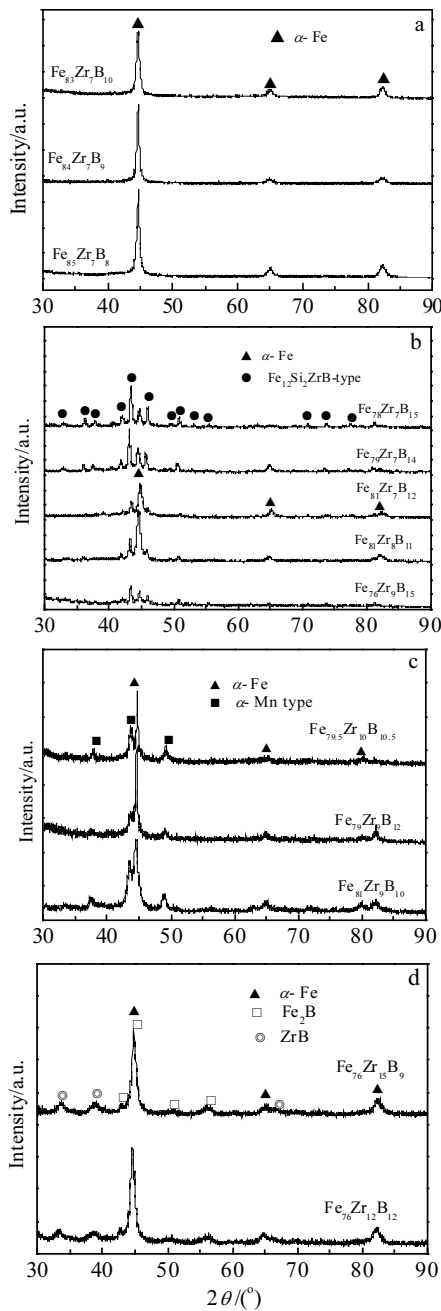


Fig.3 XRD patterns of FeZrB alloys annealed at the first crystallization temperature

Because of the great difference in atomic radius and electronegative between elements, the locations of atoms in the alloy system are easy to exchange. The formation of the different primary crystallization phases depends on the number and arrangement of neighbouring B and Zr atoms around Fe atoms. Therefore, the formation of the primary crystallization phase is quite sensitive to the composition change of alloys, and the primary crystallization phases of Fe-Zr-B alloys are listed in Table 1.

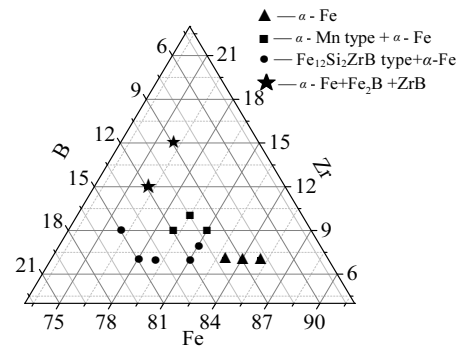


Fig.4 Diagram of primary crystallization phases for FeZrB alloys with 76 at%~85 at% Fe

Table 1 Primary crystallization phases of FeZrB alloys

Nominal composition	Primary crystallization phases
$Fe_{93-x}Zr_7B_x(x=8, 9, 10)$	$\alpha$ -Fe phase
$Fe_{93-x}Zr_7B_x(x=12, 14, 15)$ , $Fe_{81}Zr_8B_{11}$ , $Fe_{76}Zr_9B_{15}$	$\alpha$ -Fe and $Fe_{12}Si_2ZrB$ type phases
$Fe_{91-x}Zr_9B_x(x=10, 12)$ , $Fe_{79.5}Zr_{10}B_{10.5}$	$\alpha$ -Fe and $\alpha$ -Mn type phases
$Fe_{76}Zr_{12+x}B_{12-x}(x=0, 3)$	$\alpha$ -Fe, $Fe_2B$ and $ZrB$

For  $Fe_{93-x}Zr_7B_x$  ( $x=8, 9, 10$ ) alloys, only the  $\alpha$ -Fe phase with a body-centered structure precipitates from the amorphous matrix. The grain size of alloys annealed at the first crystallization temperature is 18.3, 17.9 and 15.6 nm, respectively. With increasing the B and Zr contents, different types of primary crystallization phases are observed. The formation of specific phases is associated with three following aspects<sup>[6]</sup>: similarity between local structures of the metastable and amorphous phases, high activation barriers for long range rearrangement necessary for formation of primary phases in stable supercooled liquid and surface energy. The  $Fe_{12}Si_2ZrB$ -type phase has been observed in the  $Fe_{93-x}Zr_7B_x(x=12, 14, 15)$ ,  $Fe_{81}Zr_8B_{11}$  and  $Fe_{76}Zr_9B_{15}$  alloys, and the the volume fraction of  $Fe_{12}Si_2ZrB$ -type phase is proportional to the content of B. In addition, the  $\alpha$ -Mn type phase, which is a metastable phase with a body-centered symmetry structure<sup>[19]</sup>, can be observed in  $Fe_{91-x}Zr_9B_x$  ( $x=10, 12$ ) and  $Fe_{79.5}Zr_{10}B_{10.5}$  alloys. For the  $Fe_{76}Zr_{12+x}B_{12-x}$  ( $x=0, 3$ ) alloys with the higher content of Zr and B, the primary crystallization phases are  $Fe_2B$  and  $ZrB$  phases besides  $\alpha$ -Fe phase.

The XRD patterns of  $Fe_{84}Zr_7B_9$ ,  $Fe_{78}Zr_7B_{15}$ ,  $Fe_{81}Zr_9B_{10}$  and  $Fe_{76}Zr_{12}B_{12}$  alloys annealed at the first crystallization peak temperature, which have typical primary crystallization phases, are shown in Fig.5.

TEM images of  $Fe_{84}Zr_7B_9$ ,  $Fe_{78}Zr_7B_{15}$ ,  $Fe_{81}Zr_9B_{10}$  and  $Fe_{76}Zr_{12}B_{12}$  alloys annealed at the first crystallization tem-

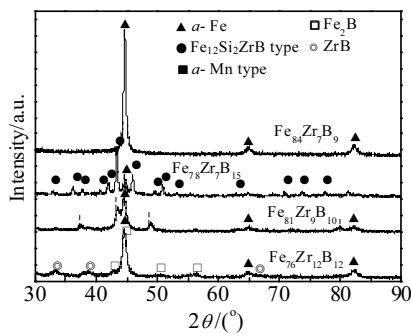


Fig.5 XRD patterns of as-quenched  $\text{Fe}_{84}\text{Zr}_7\text{B}_9$ ,  $\text{Fe}_{78}\text{Zr}_7\text{B}_{15}$ ,  $\text{Fe}_{81}\text{Zr}_9\text{B}_{10}$  and  $\text{Fe}_{76}\text{Zr}_{12}\text{B}_{12}$  alloys annealed at first crystallization temperature

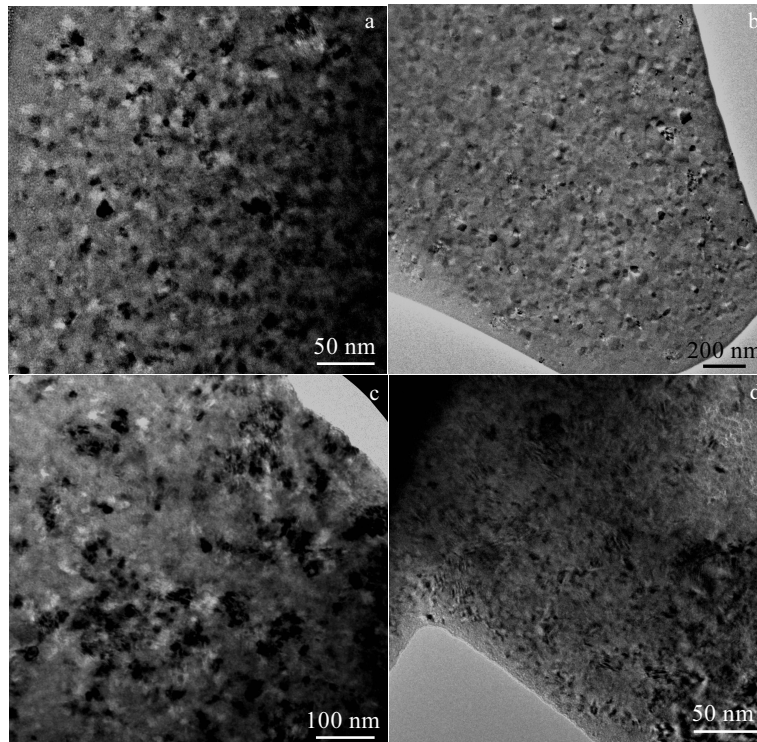


Fig.6 TEM images of  $\text{Fe}_{84}\text{Zr}_7\text{B}_9$  (a),  $\text{Fe}_{78}\text{Zr}_7\text{B}_{15}$  (b),  $\text{Fe}_{81}\text{Zr}_9\text{B}_{10}$  (c) and  $\text{Fe}_{76}\text{Zr}_{12}\text{B}_{12}$  (d) alloys annealed at first crystallization temperature

For the  $\text{Fe}_{93-x}\text{Zr}_7\text{B}_x$  ( $x=8, 9, 10$ ) alloys, the primary crystallization phase is only  $\alpha$ -Fe phase with a high crystallization volume fraction. The value of  $M_s$  is proportional to the crystallization volume fraction of  $\alpha$ -Fe phase; therefore,  $\text{Fe}_{93-x}\text{Zr}_7\text{B}_x$  ( $x=8, 9, 10$ ) alloys have the highest  $M_s$  in the present work. Moreover, the low  $H_c$  is mainly affected by the exchange-softening effect when the grain size is lower than the ferromagnetic exchange correlation length<sup>[33]</sup>. The grain size of  $\text{Fe}_{93-x}\text{Zr}_7\text{B}_x$  ( $x=8, 9, 10$ ) alloys annealed at the first crystallization temperature are all lower than the ferromagnetic exchange correlation length (approximately 20~40 nm)<sup>[34]</sup>. Therefore,

peratures are shown in Fig. 6. The morphologies are significantly different from each other. For  $\text{Fe}_{84}\text{Zr}_7\text{B}_9$  alloy (Fig.6a), the grains distributing in the amorphous matrix have the grain size in the range of 7~20 nm. For  $\text{Fe}_{78}\text{Zr}_7\text{B}_{15}$  alloy (Fig.6b), the grains are in different sizes. The grains agglomerate and distribute non-uniformly in the  $\text{Fe}_{81}\text{Zr}_9\text{B}_{10}$  alloy (Fig.6c). The grains show the irregular-shape in the  $\text{Fe}_{76}\text{Zr}_{12}\text{B}_{12}$  alloy (Fig. 6d).

The saturation magnetization ( $M_s$ ) and coercivity ( $H_c$ ) of FeZrB alloys annealed at the first crystallization temperature are given in Fig.7. Alloys with different primary crystallization phases have different magnetic properties due to their different microstructures.

$\text{Fe}_{93-x}\text{Zr}_7\text{B}_x$  ( $x=8, 9, 10$ ) alloys have the lowest  $H_c$  in the present work. For other alloys, the crystallization volume fraction of  $\alpha$ -Fe phase is lower accompanied by other crystallization phases appearing and increasing. The precipitation of different primary crystallization phases causes a change of magnetocrystalline anisotropy values and then affects  $H_c$ . For  $\text{Fe}_{93-x}\text{Zr}_7\text{B}_x$  ( $x=12, 14, 15$ ),  $\text{Fe}_{81}\text{Zr}_9\text{B}_{10}$  and  $\text{Fe}_{76}\text{Zr}_{12}\text{B}_{12}$  alloys, the primary crystallization phases contain the  $\alpha$ -Fe phase and  $\text{Fe}_{12}\text{Si}_2\text{ZrB}$ -type phase, where the  $\text{Fe}_{12}\text{Si}_2\text{ZrB}$ -type phase is a weaker ferromagnetic phase<sup>[35,36]</sup>. Therefore, the  $H_c$  of these alloys does not obviously increase even though the content of

Fe<sub>12</sub>Si<sub>2</sub>ZrB-type phase is high. For Fe<sub>91-x</sub>Zr<sub>9</sub>B<sub>x</sub>(x=10, 12) and Fe<sub>79.5</sub>Zr<sub>10</sub>B<sub>10.5</sub> alloys, the crystallization phases contain the  $\alpha$ -Fe phase and  $\alpha$ -Mn type phase, where the  $\alpha$ -Mn type phase is considered to be a metastable hard magnetic phase, and the  $H_c$  of alloys containing such phase is high<sup>[30, 36, 37]</sup>. For Fe<sub>76</sub>Zr<sub>12+x</sub>B<sub>12-x</sub>(x=0, 3) alloys, the primary crystallization phases containing the  $\alpha$ -Fe phase and the Fe<sub>2</sub>B phase which is the hard magnetic phase, resulting in the deterioration of the soft magnetic property<sup>[38]</sup>, even though the content of Fe<sub>2</sub>B phase is tiny. Overall, the relations of saturation magnetization ( $M_s$ ) and coercivity ( $H_c$ ) for the four groups of alloys with different primary crystallization phases in this work are as follows in general:  $M_{s(\alpha-Fe)} > M_{s(\alpha-Fe+\alpha-Mn \text{ type})} > M_{s(\alpha-Fe+Fe_2B+ZrB)} > M_{s(\alpha-Fe+Fe_{12}Si_2ZrB\text{-type})}$  and  $H_{c(\alpha-Fe+\alpha-Mn \text{ type})} > H_{c(\alpha-Fe+Fe_2B+ZrB)} > H_{c(\alpha-Fe+Fe_{12}Si_2ZrB\text{-type})} > H_{c(\alpha-Fe)}$ .

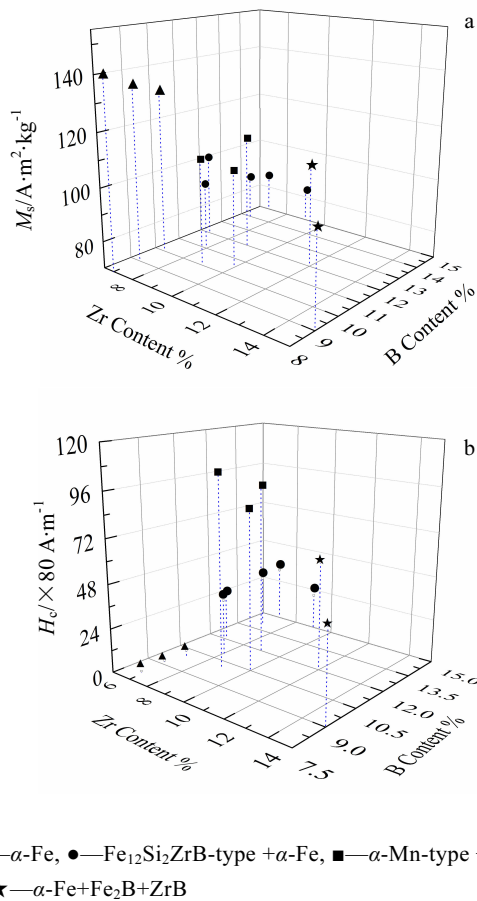


Fig.7 Saturation magnetization ( $M_s$ ) (a) and coercivity ( $H_c$ ) (b) of FeZrB alloys annealed at the first crystallization temperature

### 3 Conclusions

1) FeZrB alloys with 76 at%~85 at% Fe were prepared by melt-spinning and annealed at the first crystallization temperatures.

2) Because of the great difference values of atomic radius and electronegative between elements, the locations of atoms in the alloy system are easy to exchange. The formation of the primary crystallization phase is quite sensitive to the composition of the alloys. Four groups of primary crystallization phases are observed in the alloys with different composition, i.e.  $\alpha$ -Fe phase,  $\alpha$ -Fe+Fe<sub>12</sub>Si<sub>2</sub>ZrB-type phases,  $\alpha$ -Fe+ $\alpha$ -Mn type phases and  $\alpha$ -Fe+Fe<sub>2</sub>B+ZrB phases, and those primary crystallization phases have different morphologies.

3) The magnetic properties of alloys with different primary crystallization phases are different from each other. For the alloys with the crystallization phases containing Fe<sub>12</sub>Si<sub>2</sub>ZrB-type,  $\alpha$ -Mn type or Fe<sub>2</sub>B and ZrB phases,  $M_s$  is lower and  $H_c$  is greater, compared with those of alloys with the primary crystallization phase being only  $\alpha$ -Fe phase. The relations of saturation magnetization ( $M_s$ ) and coercivity ( $H_c$ ) for the alloys with different primary crystallization phases in this work are as follows in general:  $M_{s(\alpha-Fe)} > M_{s(\alpha-Fe+\alpha-Mn \text{ type})} > M_{s(\alpha-Fe+Fe_2B+ZrB)} > M_{s(\alpha-Fe+Fe_{12}Si_2ZrB\text{-type})}$  and  $H_{c(\alpha-Fe+\alpha-Mn \text{ type})} > H_{c(\alpha-Fe+Fe_2B+ZrB)} > H_{c(\alpha-Fe+Fe_{12}Si_2ZrB\text{-type})} > H_{c(\alpha-Fe)}$ .

### References

- Zamora J, Betancourt I. *Journal of Magnetism and Magnetic Materials*[J], 2017, 428: 165
- Lashgari H R, Chu D, Xie S S et al. *Journal of Non-Crystalline Solids*[J], 2014, 391: 61
- McHenry M E, Johnson F, Okumura H et al. *Scripta Materialia*[J], 2003, 48: 881
- Xia G T, Wang Y G, Dai J et al. *Journal of Alloys and Compounds*[J], 2017, 690: 281
- Lyasotskii I V, Dyakonova N B, Vlasova E N et al. *Phys Stat Sol (a)*[J], 2006, 203: 259
- Lyasotsky I V, Dyakonova N B, Dyakonov D L et al. *Rev Adv Mater Sci*[J], 2008, 18: 695
- Lyasotsky I V, Dyakonova N B, Dyakonov D L et al. *J Phys: Conf Ser*[J], 2008, 98: 012 026
- Dyakonova N B, Dyakonov D L, Lyasotsky I V. *Journal of Alloys and Compounds*[J], 2014, 586: S41
- Velikanova T A, Karpets M V, Kuprin V V. *Powder Metall and Met Ceram*[J], 2013, 52: 212
- Velikanova T A, Karpets M V. *Powder Metall Met Ceram*[J], 2011, 50(7-8): 479
- Velikanova T A, Karpets M V, Agraval P G et al. *Powder Metall Met Ceram*[J], 2011, 49(9-10): 606
- Chen V C, Chen C M, Su K C et al. *Mat Sci Eng A*[J], 1991, 133: 596
- Takafumi Hibino, Teruo Bitoh. *Journal of Alloys and Compounds*[J], 2017, 707: 82
- Sviridova T A, Chueva T R, Gorshenkov M V et al. *Journal of Alloys and Compounds*[J], 2016, 658: 525
- Svec P, Svec Sr P, Hosko J et al. *Journal of Alloys and*

- Compounds[J], 2014, 590: 87
- 16 Duarte M J, Kostka A, Crespo D et al. *Acta Materialia*[J], 2017, 127: 341
- 17 Takeshi N, Yukichi U. *ISIJ International*[J], 2006, 46: 1371
- 18 Sun Y M, Li B, Hua Z. *Modern Physics Letters B*[J], 2015, 29: 1 550 196
- 19 Velikanova T A, Karpets M V, Kuprin V V et al. *Powder Metall Met Ceram*[J], 2010, 49(1-2): 86
- 20 Khaenko B V, Golub S Ya, Velikanova T A et al. *Fiz Met Metalloved*[J], 1993, 75(1): 123
- 21 Ohnuma M, Sasaki O, Kuwano H et al. *Materials Transactions, JIM*[J], 1993, 34: 874
- 22 Imafuku M, Sato S, Koshihara H et al. *Scripta Materialia*[J], 2001, 44: 2369
- 23 Hirata A, Hirotsu Y, Amiya K et al. *Physical Review B*[J], 2009, 80: 140 201
- 24 Hirata A, Hirotsu Y, Amiya K et al. *Intermetallics*[J], 2008, 16: 491
- 25 Zhao B G, Kong L H, Song T T et al. *Advances in Manufacturing*[J], 2013, 1: 251
- 26 Fernández L, Barquín J C, Sal Gómez et al. *Physical Review B*[J], 2003, 329: 94
- 27 Ramakrishna Rao B, Shah A K, Srinivas M. *Metallurgical and Materials Transactions A*[J], 2011, 42 (13): 3913
- 28 Minina N A, Belousov O K, Yermishkin V A. *EPJ Web of Conferences*[J], 2011, 15: 03 006
- 29 Nagase T, Umakoshi Y, Sumida N. *Science and Technology of Advanced Materials*[J], 2002, 3(2): 119
- 30 Yu W Q, Zhou Q L, Liu Z S et al. *Journal of Materials Engineering and Performance*[J], 2017, 26: 4807
- 31 Huang H, Shao G, Tsakiroopoulos P. *Journal of Alloys and Compounds*[J], 2008, 459: 185
- 32 Hua Z, Zuo B, Wang L L et al. *Rare Metal Materials and Engineering*[J], 2015, 44(3): 616 (in Chinese)
- 33 Herzer G. *IEEE Trans Magn*[J], 1989, 25: 3327
- 34 Herzer G. *Properties and Applications of Nanocrystalline Alloys from Amorphous Precursors. NATO Science Series (Series II: Mathematics, Physics and Chemistry)*[M]. Dordrecht: Springer, 2005: 15
- 35 Xiong X Y, Muddle B C, Finlayson T R. *J Phys D: Appl Phys*[J], 2003, 36: 223
- 36 Yu W Q, Long D, Liu Y D et al. *Acta Physica Polonica A*[J], 2015, 128(3): 340
- 37 Yu W Q, Zeng H Q, Sun Y M et al. *Physics Letters A*[J], 2017, 381: 1573
- 38 Jia P, Liu J M, Wang E G et al. *Journal of Alloys and Compounds*[J], 2013, 581: 373

## FeZrB 系合金的初始晶化相及磁性能研究

于万秋<sup>1,2</sup>, 卢利平<sup>1</sup>, 左 斌<sup>2</sup>

(1. 长春理工大学 材料科学与工程学院, 吉林 长春 130022)

(2. 吉林师范大学 物理国家级实验教学示范中心, 吉林 四平 136000)

**摘要:** 采用单辊快淬法制备一系列不同名义成分的 FeZrB 合金样品, 并在第 1 个晶化峰值温度进行退火。利用同步热分析仪(STA)、X 射线衍射仪(XRD)、透射电镜(TEM)和振动样品磁强计(VSM)测试合金的热曲线、微观结构和磁性能。初始晶化相随着 FeZrB 系列合金成分比例的改变而不同。在不同成分比例的合金中观察到 4 组不同的初始晶化相, 例如  $\alpha$ -Fe,  $\alpha$ -Fe+Fe<sub>12</sub>Si<sub>2</sub>ZrB,  $\alpha$ -Fe+ $\alpha$ -Mn 和  $\alpha$ -Fe+Fe<sub>2</sub>B+ZrB。通过 TEM 观察发现具有不同初始晶化产物的合金具有不同的形貌。具有不同初始晶化产物合金的饱和磁化强度( $M_s$ )和矫顽力( $H_c$ )存在以下关系:  $M_{s(\alpha-Fe)} > M_{s(\alpha-Fe+\alpha-Mn\ type)} > M_{s(\alpha-Fe+Fe_2B+ZrB)} > M_{s(\alpha-Fe+Fe_{12}Si_2ZrB\ type)}$ ,  $H_{c(\alpha-Fe+\alpha-Mn\ type)} > H_{c(\alpha-Fe+Fe_2B+ZrB)} > H_{c(\alpha-Fe+Fe_{12}Si_2ZrB\ type)} > H_{c(\alpha-Fe)}$

**关键词:** FeZrB 合金; 初始晶化相; 微观结构; 饱和磁化强度; 矫顽力

作者简介: 于万秋, 女, 1981 年生, 博士生, 长春理工大学材料科学与工程学院, 吉林 长春 130022, 电话: 0431-85583147, E-mail: yuwanqiu2004@126.com